

Journal of Materials Chemistry A

Accepted Manuscript



This is an *Accepted Manuscript*, which has been through the Royal Society of Chemistry peer review process and has been accepted for publication.

Accepted Manuscripts are published online shortly after acceptance, before technical editing, formatting and proof reading. Using this free service, authors can make their results available to the community, in citable form, before we publish the edited article. We will replace this *Accepted Manuscript* with the edited and formatted *Advance Article* as soon as it is available.

You can find more information about *Accepted Manuscripts* in the [Information for Authors](#).

Please note that technical editing may introduce minor changes to the text and/or graphics, which may alter content. The journal's standard [Terms & Conditions](#) and the [Ethical guidelines](#) still apply. In no event shall the Royal Society of Chemistry be held responsible for any errors or omissions in this *Accepted Manuscript* or any consequences arising from the use of any information it contains.

COMMUNICATION

In-Plane and Out-of-Plane Mass Transport in Metal-Assisted Chemical Etching of GaAs

Cite this: DOI: 10.1039/x0xx00000x

Yunwon Song,^a Bugeun Ki,^a Keorock Choi,^a Ilwhan Oh^{*b} and Jungwoo Oh^{*a}

Received 00th January 2014,

Accepted 00th January 2014

DOI: 10.1039/x0xx00000x

www.rsc.org/

We have demonstrated the dependence of the metal-assisted chemical etching of GaAs on catalyst thickness. For ultra-thin (3–10 nm) Au catalysts, we found that the etch rate was significantly enhanced, an unexpected phenomenon in light of the conventional mechanism. Numerous pinholes in the metal catalyst are postulated to enable out-of-plane mass transport of reactants and products across catalyst-covered GaAs. When this process is dominant, the GaAs etch rate is facilitated and an anisotropic profile is formed. With thicker (>15 nm) Au catalysts, the conventionally known in-plane mass transport becomes dominant and lowers the etch rate with an isotropic profile. To our knowledge, this is the first report that experimentally verifies the vertical mass transport of a metal-assisted chemical etching of semiconductors. A metal-assisted chemical etching of GaAs with controlled metal catalyst thickness suggests this technique is more attractive and useful for a wide range of practical applications.

Semiconductor micro- and nano-structures with high aspect ratios are found to be versatile in a wide range of applications, such as sensors, microelectromechanical systems (MEMS)¹ and optoelectronic devices.^{2,3} To increase the performance of these devices beyond the physical limits of silicon, III-V semiconductors are being investigated as potential alternative materials for various applications. As the geometries of devices are scaled down to enhance performance, III-V devices require three-dimensional architecture to address critical challenges associated with feature size and cost-per-function issues.

Metal-assisted chemical etching is an anisotropic etching technique employing a metal catalyst and etchant solution.⁴ Since this phenomenon was discovered by Li and Bohn in 2000,⁵ it has attracted much attention due to its simple implementation and unique physical properties, with applications in various fields such as energy devices,^{6,7,8} biological sensors,⁹ membranes¹⁰ and field-effect transistors (FETs).¹¹ Generally accepted mechanisms involve

electronic hole transport into the semiconductor by reducing the oxidant using a metal catalyst and a subsequent etch of the oxidized semiconductor with an acid solution. The combined localized oxidation and etching enable high aspect ratio micro- and nano-structures,^{12,13,14} deep pores or trenches^{15,16,17} and porous semiconductors.^{10,18} Since metal-assisted chemical etching is a simple, wet-based anisotropic technique, there is no charging or crystal damage induced by the high energy plasma ions that are necessary for dry etch. A low temperature with minimal surface damage is a crucial requirement for III-V device fabrication because the damaged III-V crystal is not readily repaired by thermal annealing.

We note that most previous research on metal-assisted chemical etching has been conducted on silicon while only a few studies have addressed III-V compound semiconductors. Previous efforts to etch InP¹⁹ with conventional H₂O₂/HF showed partial success, resulting in microbumps rather than nanowires. A recent report on metal-assisted chemical etching of GaAs employing KMnO₄, a weaker oxidant than H₂O₂, successfully demonstrated periodic high aspect ratios nano-pillars by optimizing the etchant concentration and temperature.²⁰ Despite the unique benefit offered by metal-assisted chemical etching, a clear mechanism is not yet understood and potentially limits our ability to precisely tailor semiconductor structures for particular applications.

In this work, we have focused on metal catalyst thickness and its impact on the etching mechanism. We have experimentally proven in-plane and out-of-plane models for the mass transport of metal-assisted chemical etching. Etch rates and isotropic/anisotropic profiles of the top of GaAs pillars were tailored according to metal catalyst thicknesses. Reaction mechanisms strongly depend on the density of pinholes as a function of metal thickness. Etch rates and isotropic/anisotropic profiles with metal catalysts of different thicknesses can be explained by the two types of diffusion processes proposed in this work.

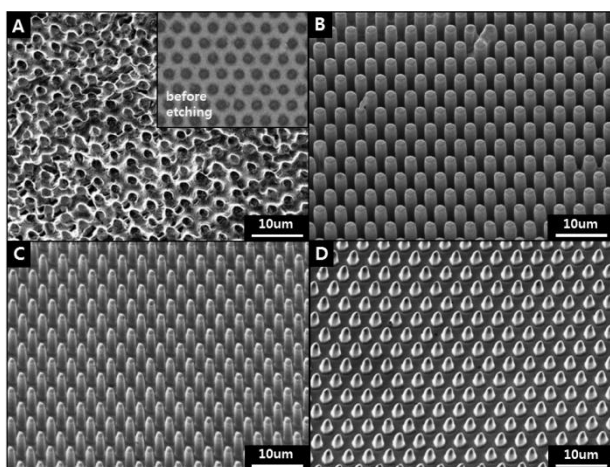


Figure 1. SEM images of metal-assisted chemical etching of GaAs with a Au catalyst of (A) 3nm, (B) 5nm, (C) 7nm, and (D) 10nm. Etch was conducted for 10 minutes in a solution of KMnO_4 and H_2SO_4 . Inset to A shows intact 3nm Au catalyst before etch.

Compound semiconductors used for metal-assisted chemical etching were Si doped n-GaAs (100) substrates with resistivity in the range of $2.4\text{--}3.3 \times 10^{-3} \Omega\text{-cm}$. GaAs substrates were pre-cleaned with conventional solvent and rinsed in de-ionized (DI) water. Periodic mesh arrays with $2 \mu\text{m}$ diameters and $2 \mu\text{m}$ spaces were formed with image reversal optical lithography. Au catalyst of various thicknesses (3, 5, 7, 10, 15, and 20nm) were then thermally evaporated on the GaAs substrates at a 2 \AA/s deposition rate under 10^{-6} Torr pressure, followed by a metal lift-off process. Before evaporation, native oxide was removed using a dilute HCl solution ($\text{HCl}:\text{H}_2\text{O}=1:1$) and substrates were thoroughly cleaned in a DI rinse.

The etch solution was prepared by dissolving potassium permanganate (KMnO_4) with DI water and stirred for 30 minutes. Then 37mM KMnO_4 was mixed with sulfuric acid (H_2SO_4). Samples were etched for designated durations (3, 5, or 10 minutes) at $50\text{--}53^\circ\text{C}$. Etching was stopped by thoroughly rinsing with DI water and drying in a N_2 stream. The height of the etched pillars was measured using field emission scanning electron microscopy (FE-SEM).

Figure 1 shows scanning electron microscopy (SEM) images of metal-assisted chemical etching of GaAs with a Au catalyst. Etch was conducted for 10 minutes on a Au mesh pattern on a GaAs substrate with different Au catalyst thicknesses of (A) 3nm, (B) 5nm, (C) 7nm and (D) 10nm. Note that the inset in A shows an intact 3nm Au catalyst on a GaAs substrate in circular mesh arrays before etch. The catalyst dimension was fixed at mesh arrays with $2 \mu\text{m}$ diameters and spaces to prevent the etching rate from changing with pattern size, not metal thickness, at the thick metal region.²¹

With an ultra-thin Au catalyst of 3nm (Figures 1A), etch was not successful. The Au catalyst did not maintain its initial periodic structure, but seemed to be rearranged and peeled off the GaAs substrate at some sites, probably because Au catalyst loses its anchor with the underlying substrate and becomes mobile during the etch process. High-resolution images of the Au catalyst in Figure 4 will shed more light on this phenomenon. On the other hand, a GaAs etch with a thicker Au catalyst of 5 nm (Figure 1B) produced dramatically different results. In this case, high aspect ratio GaAs pillars were fabricated in circular mesh arrays. Compared with the 3nm

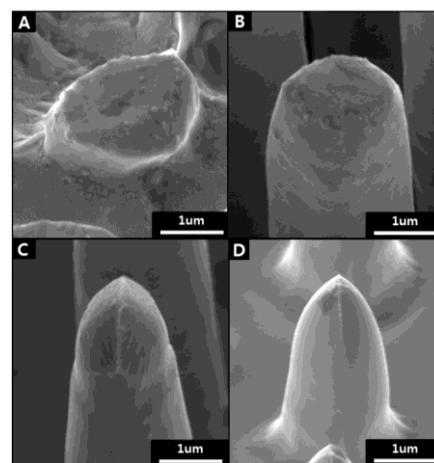


Figure 2. SEM images of the top of the GaAs pillar after etch for 10 minutes with a Au catalyst of (A) 3nm, (B) 5nm, (C) 7nm, and (D) 10nm.

thick Au catalyst, the 5nm Au catalyst accelerated the vertical etch rate and produced high aspect ratio GaAs pillars. As the Au catalyst thickened to 7nm (Figure 1C) and 10nm (Figure 1D), etch still produced the GaAs pillars. However, the etch rate with a thicker Au catalyst was much slower than the one with a 5nm thickness. With a peak etch rate recorded at 5nm, the etch rate gradually decreased as the Au catalyst became thicker.

With Au catalyst thickness, another point worth noting is the transition of anisotropic/isotropic characteristics. Figure 2 compares the top portion of GaAs pillars with 3, 5, 7, and 10nm thick Au catalyst after etch for 10 minutes. With the 3 and 5nm Au catalyst, the GaAs pillar exhibited a cylindrical top, indicating anisotropic etch characteristics. As the Au catalyst increased to 7 and 10nm thick, the top of the GaAs pillars became conical with a smaller pillar diameter at the bottom, indicating more isotropic etch characteristics. This transition toward isotropic etch is probably caused by excess hole diffusion towards the bare GaAs region. This point will be

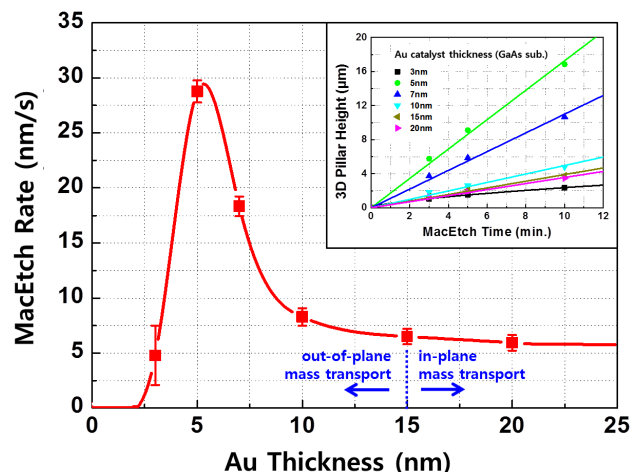


Figure 3. Out-of-plane and in-plane mass transport regimes defined by variations in etch rates as a function of Au catalyst thickness. Inset shows the pillar height measured over time for different Au catalyst thicknesses.

detailed below.

Figure 3 shows etch rate as a function of Au thickness. The inset shows pillar height measured over time for different Au catalyst thicknesses. When the Au catalyst was 3nm thick, an accurate rate was difficult to measure because of the poorly defined GaAs pillars. Wide error bars with a low etch rate indicate unsuccessful metal-assisted chemical etching of the GaAs. After increasing the Au catalyst to 5nm, the etch rate increased dramatically to as high as 29 nm/s. This increase is interpreted to be the result of enhanced mass transport for the chemical reaction, which will be clarified below. For the 7nm Au catalyst, the etch rate began to roll-off. When the Au catalyst was 10nm thick, etch rates further decreased to 8nm/s. For Au thicknesses ≥ 15 nm, etch rate was saturated and essentially became independent of Au thickness. From the results, metal-assisted chemical etching of GaAs with different Au catalyst thicknesses can be classified into two regimes: out-of-plane mass transport and in-plane mass transport. These regimes are directly related to the physical properties of the Au catalyst.

At this point, the metal-assisted chemical etching of GaAs exhibits different behaviour from that of Si. For Si, with a thin (<10nm) catalyst layer with pinholes, etching beneath the catalyst layer is non-uniform, forming nanowires or nanoflakes through the pinholes²¹. However, for GaAs, no such nanoflake or nanowire formation with a thin catalyst layer is observed in our experiment or in a previous report²⁰. The reason for the difference is currently unclear. We tentatively attribute this difference to material properties. That is, whereas Si is relatively insoluble and forms a rigid oxide, GaAs is known to be more soluble with weaker oxide.

To elucidate the etch mechanism in more detail, high-resolution images of the Au catalyst surface were taken. SEM images in Figure 4 compare its surface morphology (A=3nm, B=5nm, C=7nm, D=15nm) observed after etch for 3min. As a reference, the inset in Figure 4A was 3nm thick Au catalyst before etch and its surface were relatively intact and smooth. However, after etching, different morphologies of the Au catalyst were observed. As shown in in Figure 4A, the Au catalyst layer seems to coalesce with several wide holes. The

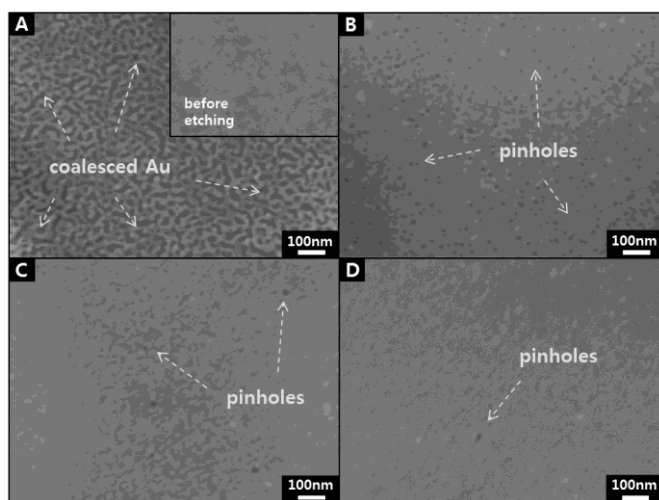
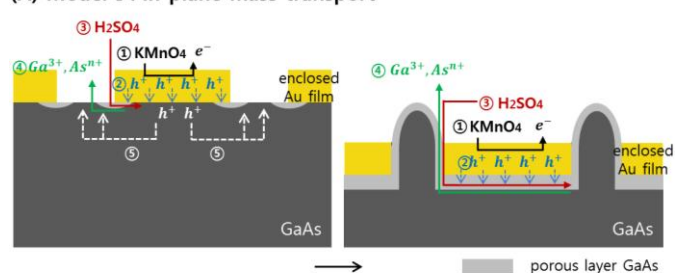


Figure 4. Comparison of the surface morphology of Au catalyst (A=3nm, B=5nm, C=7nm, D=10nm) after etch for 3min. As a reference, the inset in A shows seamless 3nm thick Au catalyst before etch.

(A) Model-I : in-plane mass transport



(B) Model-II : out-of-plane mass transport

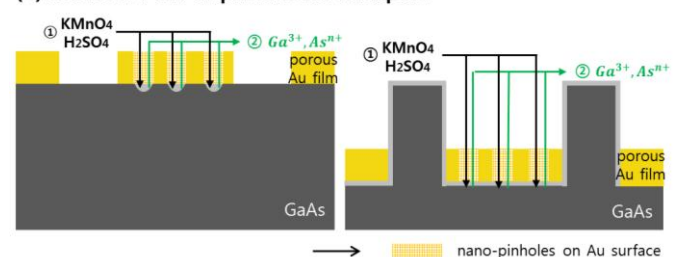


Figure 5. Schematic illustration of (A) Model-I: widely accepted in-plane mass transport and (B) Model-II: proposed out-of-plane mass transport of reactant and product in metal-assisted chemical etching.

unsuccessful GaAs etch in Figure 1A is attributed to the collapse of the Au catalyst due to wide holes distributed in the ultra-thin film. Figure 4B refers to the results with 5nm thick Au. Unlike the ultra-thin 3nm Au catalyst, the structural integrity of the Au catalyst layer is maintained even though numerous nano-sized pinholes are observed.

Coalesced Au and nano-pinholes were results of a dynamic redistribution of Au from cyclic reaction forming Au^{3+} and back to Au^0 , as explained in the following paragraph on etch mechanisms.²² The repeated etching and deposition processes transfer Au to an adjacent catalyst region similar to a nucleation effect. The highest GaAs etch rate measured with 5nm thick Au is related to the presence of nano-pinholes. Pinholes allowed out-of-plane mass transport of the reactant and product during etch. As the Au thickness increased to 7nm (Figure 4C) and 10nm (Figure 4D), the number of pinholes decreased substantially. Etch rate roll-off is in good agreement with of the fewer pinholes. When Au thickness was 15nm, almost seamless surface morphology was observed without any pinholes in any given area. For Au thicknesses ≥ 15 nm, the saturated etch rate coincides with the surface morphology of the Au catalyst.

In previous reports, proposed mechanisms for metal-assisted chemical etching can be roughly classified into two categories: in hole injection mechanisms, the metal catalyst reduces the oxidant ($KMnO_4$ in current work), producing free electronic holes. Electronic holes are injected into the valence band of the semiconductor and oxidize it. Then an etchant (H_2SO_4 in current work) dissolves the oxidized semiconductor. On the other hand, in the more recently proposed metal catalysis mechanism²², the metal catalyst is oxidized by oxidant and dissolved into a solution. Then the dissolved metal ion redeposits onto the semiconductor and etches it. Whereas the hole injection model assumes semiconductor band control for the metal-assisted chemical etching, the metal catalysis model assumes a simple heterogeneous surface reaction.

In both mechanisms, the dissolved semiconductor ions need to diffuse out from the metal/semiconductor interface into the

bulk solution. Figure 5A illustrates model-I for the in-plane mass transport of reactant and product. Note that in this model, the etch rate is independent of catalyst thickness, because the catalyst layer is thick and uniform and mass transport of reactants and products is virtually blocked through the metal layer, occurring only at the edge of the metal/semiconductor interface. Etch rate is relatively low because of in-plane mass transport. On the other hand, Figure 5B is a schematic illustration of the out-of-plane model-II that we have experimentally proven for the first time. In this model, electrochemically generated nano-pinholes in the metal catalyst not only enhance important catalytic effects in redox reactions,^{23,24} but also act as a diffusion pathway for the reactants (H₂SO₄) and products (Ga³⁺ and Asⁿ⁺ ions) for chemical etching oxidized GaAs. When diffusion through the pinholes is the dominant mass transport process, the chemical reaction uniformly occurs at any location beneath the metal catalyst. Therefore, the conical top of the pillar was not observed as a result of homogeneous etching at the Au/GaAs interface. In addition, the overall etch rate is enhanced and the cylindrical top of the pillar is formed. The density of pinholes in the metal catalyst is determined by the metal thickness. This model supports that the etch rate has a strong dependence on Au thickness ranging from 3 to 10nm and is independent of Au thickness ≥ 15 nm in terms of pinhole density.

With these two models, experimental results can be interpreted consistently. When Au thickness ≥ 15 nm, the conventional model-I becomes the dominant process and the etch approaches the edge of the Au/GaAs interface, which results in a low etch rate and isotropic and conical profiles. For a 7~10 nm Au catalyst, the etch make a transition from model-I to model-II as the number of pinholes decreases. The highest etch rate and cylindrical top of the GaAs pillars are driven by model II because of the numerous pinholes in 5nm Au catalyst. A 3nm Au catalyst is too thin to transport sufficient electronic holes in the GaAs, resulting in a scattered etch rate.

Conclusions

Metal-assisted chemical etching of GaAs has a strong dependency on surface porosity or the thickness of the metal catalyst. Several pinholes formed in the 5nm Au catalyst facilitated the GaAs etch rate to as high as 29 nm/s, while the 15~20nm Au catalyst lowered the GaAs etch rate substantially. We have proven with out-of-plane models for metal-assisted chemical etching of GaAs that pinholes in thin metal serves as diffusion pathway for the reactant and product during the catalytic reduction of oxidant in the chemical etching of GaAs. With thin Au and mass transport occurring through pinholes, metal-assisted chemical etching of GaAs was enhanced with high anisotropic etch profiles. With thick Au, however, metal-assisted chemical etching of GaAs showed little dependency on Au thickness, suggesting in-plane mass transport.

Acknowledgements

This research was supported by the Ministry of Science, ICT and Future Planning (MSIP), Korea, under the IT Consilience Creative Program (NIPA-2014-H0201-14-1002) supervised by the National IT Industry Promotion Agency (NIPA). This research was supported by the Basic Science Research Program through the National Research Foundation of Korea (NRF) funded by the Ministry of Education, Science and Technology (2013R1A1A2012111 and 2012R1A1A1012933).

Notes and references

^a School of Integrated Technology, Yonsei University, 85 Songdogwahak-ro, Yeonsu-gu, Incheon, 406-840, Republic of Korea. E-mail: jungwoo.oh@yonsei.ac.kr

^b Department of Applied Chemistry, Kumoh National Institute of Technology, 1 Yanggo-dong, Gumi, 730-701, Republic of Korea. E-mail: ioh@kumoh.ac.kr

- M. J. Madou, *Fundamentals of microfabrication*, CRC Press, Boca Raton, Fla, USA, 1997
- R. Yan, D. Gargas, P. Yang, *Nat. Photon.*, 2009, **3**, 569
- K.Q. Peng, S.T. Lee, *Adv. Mater.*, 2011, **23**, 198
- Z. Huang, N. Geyer, P. Werner, J. De Boor, U. Gösele, *Adv. Mater.*, 2011, **23**, 285
- X. Li, P.W. Bohn, *Appl. Phys. Lett.*, 2000, **77**, 2572
- P. K. Mohseni, S. H. Kim, X. Zhao, K. Balasundaram, J. D. Kim, L. Pan, J. A. Rogers, J. J. Coleman, X. Li, *J. Appl. Phys.*, 2013, **114**, 064909
- J. C. Shin, D. Chanda, W. Chern, K. J. Yu, J. A. Rogers, X. Li, *IEEE J. Photovoltaics*, 2012, **2**, 129
- E. C. Garnett, P. Yang, *J. Am. Chem. Soc.*, 2008, **130**, 9224
- M.-L. Zhang, C.-Q. Yi, X. Fan, K.-Q. Peng, N.-B. Wong, M.-S. Yang, R.-Q. Zhang, S.-T. Lee, *Appl. Phys. Lett.*, 2008, **92**, 043116
- S. Cruz, A. Hönig-d'Orville, J. Müller, *J. Electrochem. Soc.*, 2005, **152**, C418
- K.-J. Moon, J.-H. Choi, T.-I. Lee, M.-H. Ham, W.-J. Maeng, I. Hwang, H. Kim, J.-M. Myoung, *Microelectron. Eng.*, 2010, **87**, 2407
- K. Balasundaram, J. S. Sadhu, J. C. Shin, B. Azeredo, D. Chanda, M. Malik, K. Hsu, J. A. Rogers, P. Ferreira, S. Sinha, X. Li, *Nanotechnology*, 2012, **23**, 305304
- K. Peng, Y. Xu, Y. Wu, Y. Yan, S.-T. Lee, J. Zhu, *Small*, 2005, **1**, 1062
- Z. Huang, H. Fang, J. Zhu, *Adv. Mater.*, 2007, **19**, 744
- C.-L. Lee, K. Tsujino, Y. Kanda, S. Ikeda, M. Matsumura, *J. Mater. Chem.*, 2008, **18**, 1015
- C. Chartier, S. Bastide, C. Lévy-Clément, *Electrochim. Acta*, 2008, **53**, 5509
- K. Rykaczewski, O. J. Hildreth, C. P. Wong, A. G. Fedorov, J. H. J. Scott, *Nano Lett.*, 2011, **11**, 2369
- A. I. Hochbaum, D. Gargas, Y. J. Hwang, P. Yang, *Nano Lett.*, 2009, **9**, 3550
- H. Asoh, T. Yokoyama, S. Ono, *Jpn. J. Appl. Phys.*, 2010, **49**, 046505
- M. DeJarld, J. C. Shin, W. Chern, D. Chanda, K. Balasundaram, J. A. Rogers, X. Li, *Nano Lett.*, 2011, **11**, 5259
- N. Geyer, B. Fuhrmann, Z. Huang, J. De Boor, H. S. Leipner, P. Werner, *J. Phys. Chem. C*, 2012, **116**, 13446
- Z. R. Smith, R. L. Smith, S. D. Collins, *Electrochim. Acta*, 2013, **92**, 139
- L. A. Harris, J. A. Hugo, *J. Electrochem. Soc.*, 1981, **128**, 1203
- M. Szklarczyk, J. O'M Bockris, *J. Phys. Chem.*, 1984, **88**, 1808